Inviscid Stability of Nearly Parallel Flows

As Re → ∞, the OS equation simplifies to the Rayleigh equation:

$$\varphi_{yy} - \left(\alpha^2 + \frac{1}{U-c} U_{yy}\right)\varphi = 0 \quad (1)$$

And only $\varphi = 0$ at two locations can be enforced. Note that U(y) may be viscous in origin; however, the stability determined via (1) is for Re → ∞ thus neglects the effects of viscosity.

For flows with walls at $y = y_1$ & y_2
$u = 0$ ie $\varphi = 0$ at y_1 & y_2

$c(\alpha)$ = eigenvalue & eigenfunction
Since i not in equation then complex conjugate shows that $c^*(\alpha)$ & α^* are correspondg solutions with negative c_i: each growing mode has correspondg decaying mode. Stable solutions can only have $c = c_r$, which is true only for Rayleigh equation since OS equation includes i

Stability of $U(y)$ investigated subject Rayleigh equation and normal mode disturbances, which obey inviscid dynamics. However $U(y)$ can be any profile, eg, viscous flow solutions for Couette, Poiseuille, Blasius flows etc.

Rayleigh proved (for $\mu = 0$:

(1) Point of inflection theorem: a necessary but not sufficient condition for inviscid instability is U(y) has an inflection point: $U_{yy} = 0$. Thus, U(y) without inflection points is stable such as Poiseuille flow, plane Couette flow, and Blasius boundary layer and all boundary layers with favorable pressure gradients.

(2) Fjortoft theorem: a stronger additional necessary but not sufficient condition for inviscid instability is that if the velocity at the infliction point is U_I than if $U_{yy}(U-U_I) < 0$ somewhere in the flow it is unstable.

Appendix A provides proofs for (1) and (2).

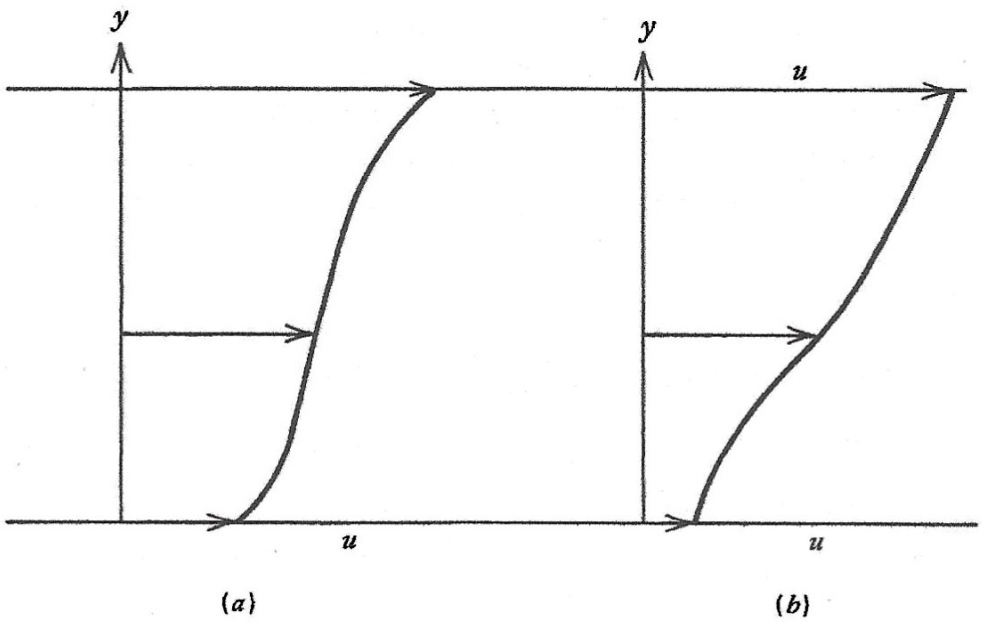

Figure 25.3 Inviscid instability of shear flows. Both cases are possibly unstable by Rayleigh's theorem, but only (*b*) is possibly unstable by Fjørtoft's theorem.

Theorem (2) concerns the neutral stability mode with $C_I = 0$. For this mode $C = C_R$ and $U - c$ is real such that C_R must lie between the minimum and maximum values of U(y) and $U - c = 0$ at some point within the flow. This point is called the critical layer because the Rayleigh equation is singular at this location. $U = C_R$ at the critical layer.

It should be recognized that the inviscid eigenfunctions $\varphi(y)$ can not be uniformly valid as two boundary conditions $\varphi_{y=0}$ have been dropped along with the non-uniformity caused by the critical layer, whereas the OS equation has no issues at this point. Lin (1945) showed that when a profile has an inflection point the critical layer is at this point.

Rayliegh equations can be solved both analytically or numerically; however, singularity on real axis at $c = c_r = U$.

Both theorems are for $\mu = 0$ & necessary but not sufficient

Conclusion: BL with adverse pressure gradient & free shear flows (mixing layers, jets, wakes) are potentially unstable

vs. Couette & Poiseuille & BL with zero or favorable pressure gradient which have no inflection point are stable in inviscid limit

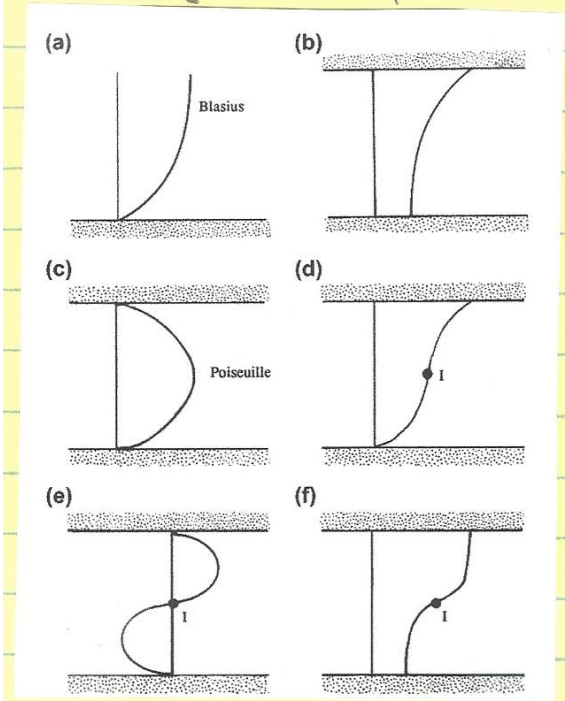

(a), (b), (c) no I

(d) has I, but

only (e) & (f)

Satisfy $U_{yy}(U - U_I) < 0$

Critical layers

Howards semi circle theorem:

$U_{min} < c_r < U_{max}$

Since growing/decaying modes are characterized by $c_i \neq 0$ & neutral modes $c = c_r$

$\therefore$ neutral modes have $U = c = c_r$ @ y_c

where y near y_c called critical layer

At $U = c$ highest derivative Rayleigh equation drops out & eigenfunction solutions are discontinuous, which is not the case for the full Orr-Sommerfeld equation due to the effects of viscosity.

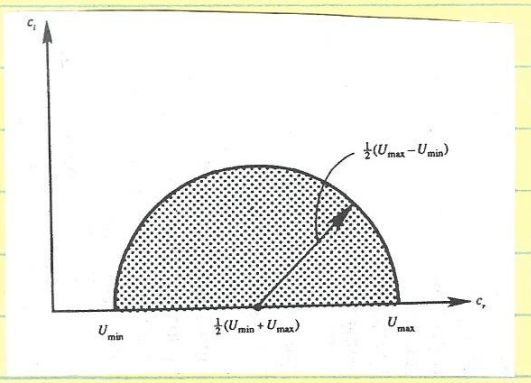

$c = c_r + i c_i$ must lie within semi circle shown

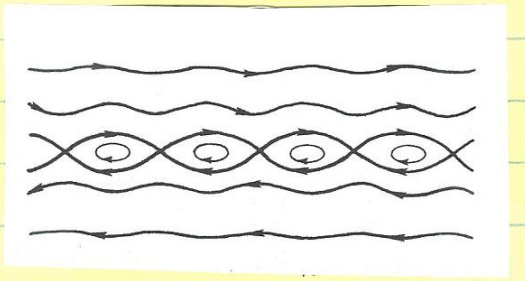

Kelvin cat's eye pattern near critical layer

Viscous Stability of Nearly Parallel Flows

Intuitively one would expect viscosity to be stabilizing, as per Taylor vortices; however, in actuality viscosity can in some cases be destabilizing, e.g., Poiseuille and Blasius profiles do not have inflection points such that are inviscidly stable, yet these flows undergo transition to turbulence for sufficiently large Re, which suggest that viscous effects are destabilizing.

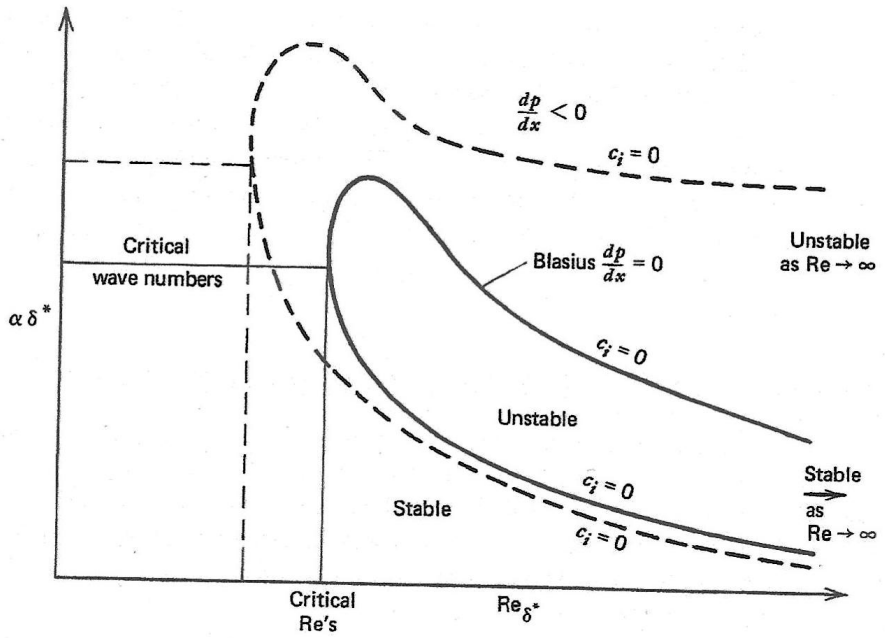

Figure 25.4 General shape of the neutral stability curve (locus of $c_i = 0$ in wavenumber–Reynolds number space) for a Blasius boundary layer and for layers with adverse pressure gradients.

1. Neutral stability (thumb) curve divides α-Re plane into stable vs. unstable regions.
2. For small Re, the flow is stable to disturbances of all wave numbers due to viscous damping, whereas for infinite Re the flow is stable as per Rayliegh point of inflection theorem.
3. However, within the thumb curve is a range of wavenumbers for which the flow is unstable called Tollmien-Schlicting (TS) waves.

4. The critical point is the point on the thumb curve with the smallest Re, which for the Blasius boundary layer is $Re = \frac{U\delta^*}{\nu} = 520$ with TS wavenumber $\alpha\delta^* = 0.3$ and wavelength $L = \frac{2\pi}{\alpha} = \frac{2\pi\delta^*}{0.3} \approx 18\delta^* \approx 6\delta$. Thus, the first unstable wave has a very long wavelength, and the boundary layer is stable subject short-wave lengths.
5. As the boundary layer grows the Re increases and the band of unstable wavelengths becomes larger. Note that the boundary layer never reaches infinite Re as the end result of the previous instability is turbulent flow.

For adverse pressure gradients the boundary layer profiles have inflection points and thus are inviscid unstable such that the upper branch of the neutral stability curve has a finite limit for infinite Re. Most importantly, the critical Re is reduced and the range of unstable wavenumbers is increased, i.e., adverse pressure gradients promote turbulence transition.

Table 25.1 Critical Reynolds Number for Falkner–Skan Boundary Layers

β_1	1	0.8	0.6	0.5	0.4	0.3	0.2
m	1	0.667	0.429	0.333	0.250	0.176	0.111
$H = \delta^*/\theta$	2.216	2.24	2.274	2.297	2.325	2.362	2.411
Re_crit	12490	10920	8890	7680	6230	4550	2830
β_1	0.1	0.05	0	−0.05	−0.1	−0.14	−0.1988
m	0.053	0.026	0	−0.024	−0.048	−0.065	−0.0904
$H = \delta^*/\theta$	2.481	2.529	2.591	2.676	2.801	2.963	4.029
Re_crit	1380	865	520	318	199	138	67

Recall Falkner-Skan m = 1 is stagnation, m = 0 is the Blasius, and m = -0.0904 is separation profiles with corresponding large, medium and small Re critical values, which can be used as rough estimates for arbitrary profiles with similar H. The accuracy is better for favorable vs. unfavorable pressure gradients.

As another example consider the neutral stability curve for a shear layer profile U = tanh(y/L), which is a shear layer making a transition from U_1 to U_2 a seen by an observer moving at $(U_1+U_2)/2$.

The profile is only stable for Re = 0 for all wave numbers.

For infinite Re the flow is unstable to long wavelengths $0 \leq \alpha L \leq 1$, which is the Kelvin-Helmholtz instability.

A new aspect is that for wavelengths shorter than the shear layer thickness L the shear layer is stable. Between these extremes of Re the neutral stability curve varies monotonically. Viscosity has a purely stabilizing effect on this flow.[1]

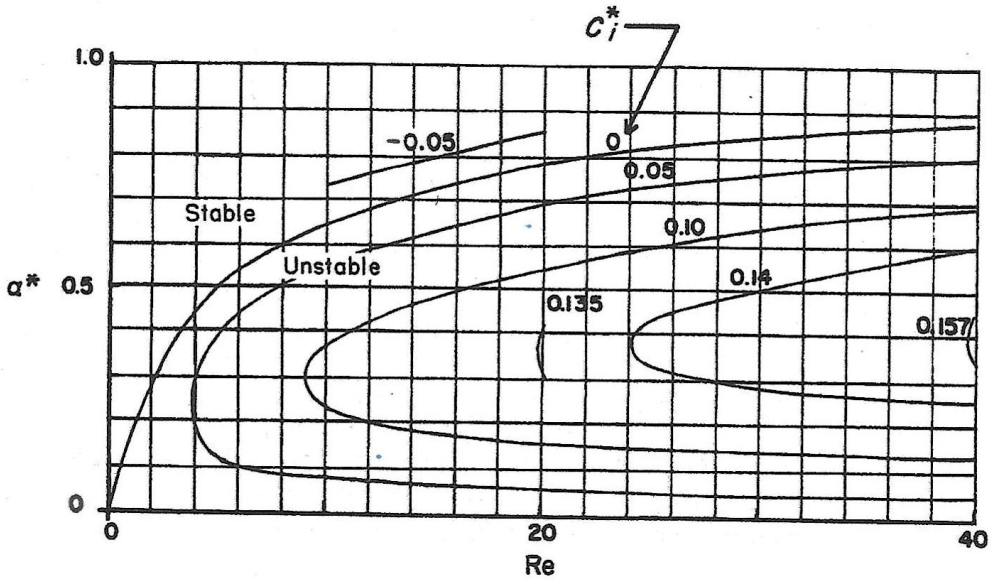

Figure 25.5 Curves of constant amplification $c_i^* = c_i \alpha L/U_0$ in the wavenumber $\alpha^* = \alpha L$ versus Re plane for a shear layer $u = U_0 \tanh(y/L)$. Neutral stability is given by $c_i^* = 0$. Viscosity makes the flow completely stable only at Re = 0. Reproduced with permission from Betchov and Szewczyk (1963). Graph courtesy of A. Szewczyk, Notre Dame University.

[1]Alternate description: At all Re the flow is unstable to waves having low wave numbers in the range $0 < k < k_u$, where the upper limit depends on Re. For high Re, the range of unstable wave numbers increases to $0 < k < L^{-1}$, which corresponds to wavelength range $\infty > \lambda > 2\pi L$, i.e., long wavelength instability. In the limit of kL $\rightarrow$ 0 the results simplify to a vortex sheet.

(1) Profiles with inflection points (first three in table below) have small Re critical and insensitivity to the detailed shape of U(y). (2) Profiles without inflection points are stable for infinite Re (the other profiles in the table below) and have larger Re critical with sensitivity to the detailed shape of U(y). (3) The last two profiles in the table according to linear stability theory are completely stable, which is an obvious failure of the theory.

Table 25.2 Stability Characteristics

Flow	$U(y)/U_0$	$U_0L/v = \mathrm{Re}_c$	$\alpha_c L = \alpha^*$	$0 - \alpha^*_\infty$ Inviscid	Remarks
Shear layer	$\tanh(y/L)$	0	0	0–1.0	Kelvin–Helmholtz, Re $\to \infty$
Jet	$\mathrm{sech}^2(y/L)$	4	0.2	0–2.0	Even mode
Falkner–Skan separating profile	$\beta = -0.199$	64	1.24	0–0.8	$L = \delta^*$
Blasius	$\beta = 0$	520	0.30	0	$L = \delta^*$
Stagnation	$\beta = 1$	14,000		0	$L = 8^*$
Flow into a sink	$\beta \to \infty$	21,700	0.17	0	$L = \delta^*$
Poiseuille (plane)	$1 - (y/L)^2$	5,780	1.02	0	L = half-width
Poiseuille (cylindrical)	$1 - (r/R)^2$	∞		0	Stable
Couette (plane)	y/L	∞		0	Stable

Linear Stability Theory (LST), which relies on small perturbations growing via viscous mechanisms (Tollmien-Schlichting waves), works well for boundary layers because they develop in space and have a clear inflection point or "health" (shape factor) that leads to gradual instability.

Conversely, in Plane Couette flow (shear between two moving plates) and Plane Poiseuille flow (pressure-driven channel flow), LST fails to accurately predict the low Reynolds numbers at which they transition to turbulence. This is because these flows are primarily unstable to finite-amplitude perturbations rather than infinitesimally small ones, driven by a non-modal mechanism known as "bypass transition."

Experiments for Blasius Boundary Layers

Advancements in fluid mechanics have normally advanced from observation to experiments to analysis and theory. However, the linear stability theory for nearly parallel flows, i.e., TS waves and the neutral stability curve lacked validation for many years.

The Blasius BL is known to become turbulent for $Re_{\delta^*} \approx 3000$; however, since unstable waves grow slowly Re_{δ^*} critical is only 520. Moreover, 2D TS waves are only the first stage of a complex process evolving from 2D to 3D to nonlinear processes and final transition to turbulence. Idealized transition, as per linear theory is called natural transition, whereas in most cases large disturbances induce transition that bypass natural transition.

A special wind tunnel with very low levels of free stream turbulence (rms fluctuations < .03%) was built by the National Bureau of Standards ca. 1947 for the study of natural transition, which used a vibrating ribbon to generate TS waves.

Fig 25.6 shows the data with early approximate (Re_{δ^*} = 450) and later exact (Re_{δ^*} =520) OS solutions. The ordinate is the disturbance frequency $\omega = \alpha c_R$ as experimentally easier to determine. Differences are attributed to growth of the BL and effects of weak adverse pressure gradient near Re critical. Note $Re = Re_{\delta^*}$.

Fig 25.7 shows more recent experiments and simulations, which provide confirmation the OS equation. Note $Re = \sqrt{U_0 x/\nu}$.

Fig 25.8 shows sketch of the TS wave flow pattern. Fig 25.9 shows downward view of the TS waves including formation of Λ-shaped structures. Fig 25.10 shows TS waves as cylindrical bands.

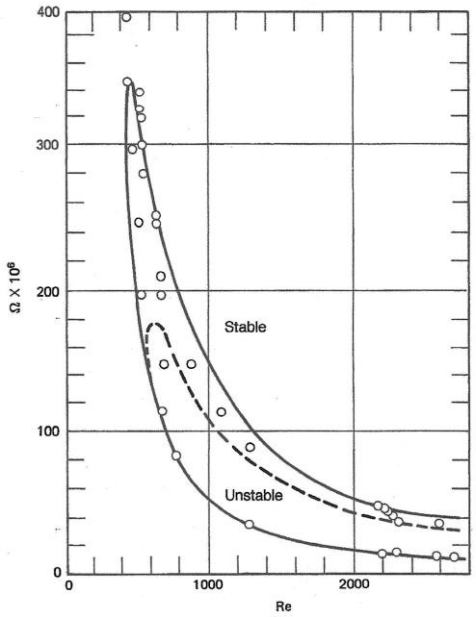

Figure 25.6 Blasius boundary layer neutral stability curves, $C_i = 0$, in the wavenumber–Re plane. Experimental points, Schubauer and Skramstad (1947); solid line, Shen (1954); dashed line, Schlichting (1933). $\mathrm{Re} = U\delta^*/\nu$ and $\Omega = \alpha c_r/\mathrm{Re}$.

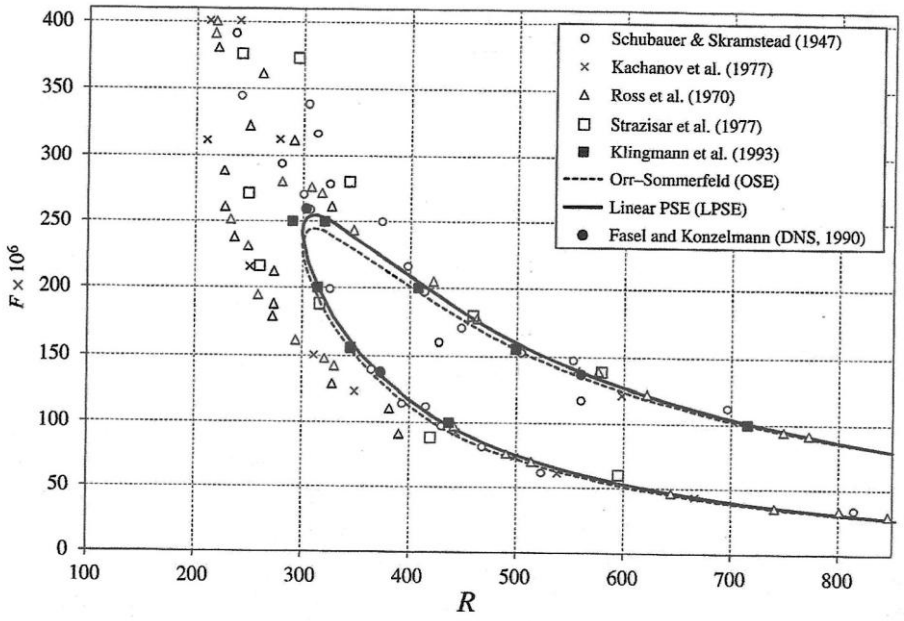

Figure 25.7 Modern Blasius boundary layer results from Saric (2013); $F = 2\pi f\nu/U_0^2 \times 10^6$ and $R = \sqrt{U_0 x/\nu} = \sqrt{\mathrm{Re}_x}$. Solid line is parabolized stability equations (PSE) calculations from Bertolotti et al. (1992) Dashed line is solution of the Orr–Sommerfeld equation (OSE) from Wazzan et al. (1968). The [•] symbols are direct numerical simulation (DNS) calculations of Fasel and Konzelmann (1990). Experimental results are Schubauer and Skramstead (1947) [◦], Ross, Barnes, Burns, and Ross (1971) [△] Kachanov et al. (1977) [×], Strazisar et al. (1977) [□] and Klingmann et al. (1993) [■]

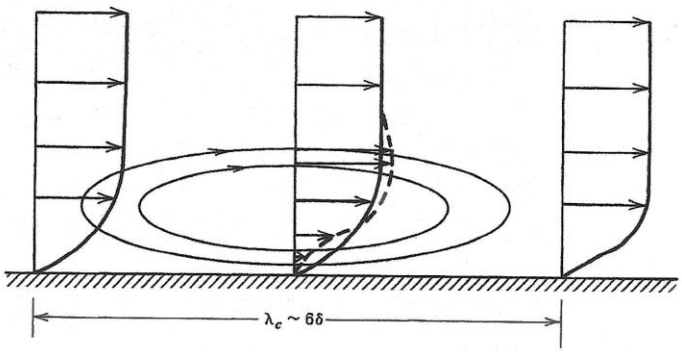

Figure 25.8 Flow pattern in the critical TS wave. Perturbation streamlines are given in a coordinate system moving with the wave.

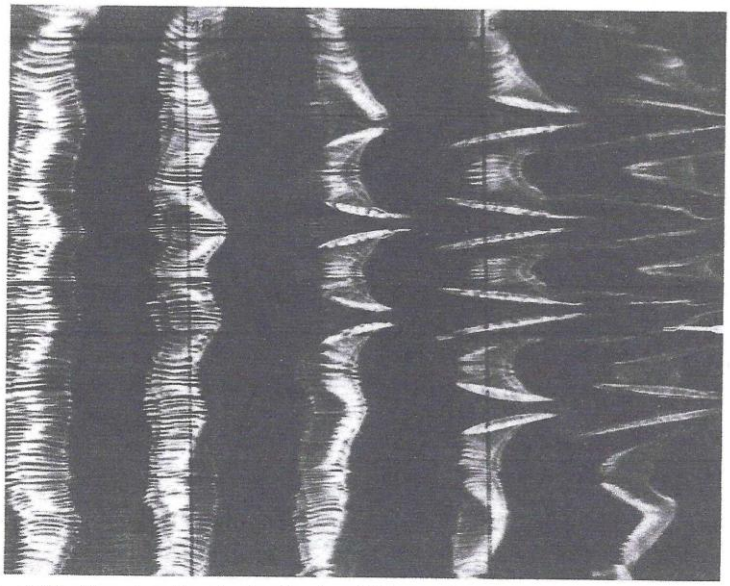

Figure 25.9 Plan view of smoke visualization of TS waves in a Blasius boundary layer. Flow is left to right. Note the development of three-dimensional secondary instabilities. Courtesy of A. Thomas, Lockheed-Georgia Co. See Thomas (1983).

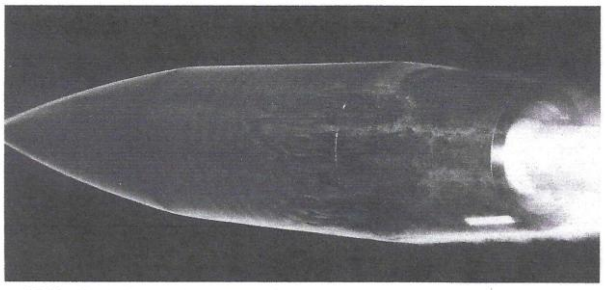

Figure 25.10 Smoke in the flow over a cylindrical body shows natural transition. The TS waves (light–dark bands) form A shapes that ultimately break down. Courtesy of T. J. Mueller and R. C. Nelson, University of Notre Dame. Reprinted with permission.

Transition, Secondary Instability, and Bypass

Wall turbulence transition is in fact a very complex, which is summarized by a Morkovin Map, as per Fig 25.12. Constructed for BL but more generally useful other wall turbulence flows. Categories and nomenclature under continuous development and important for conceptual consensus.

The map starts with the base flow and proceeds to the location and types of disturbances at the next level. Although not yet included explicitly, the disturbance strength is a very important parameter.

Right side path covers natural transition, including primary (TS waves etc.) and secondary/tertiary instabilities (Λ-shaped structures/hairpin vortices) with various arrangements (aligned vs. staggered). Ultimately a very rapid breakup of these 3D structures results in self-sustaining turbulence.

Left side path covers bypass transition associated with stronger amplitude disturbances.

Center path covers transient growth, which is relevant Couette and Poiseuille flows.

Shaded vertical lines indicate possibility movement laterally between categories.

After a sequence of instabilities turbulent spots are formed, which grow laterally and longitudinally and swept downstream amalgamating and ultimately resulting in fully turbulent flow. All the above strongly depends on wall rough ess, pressure gradient, free stream turbulence etc.

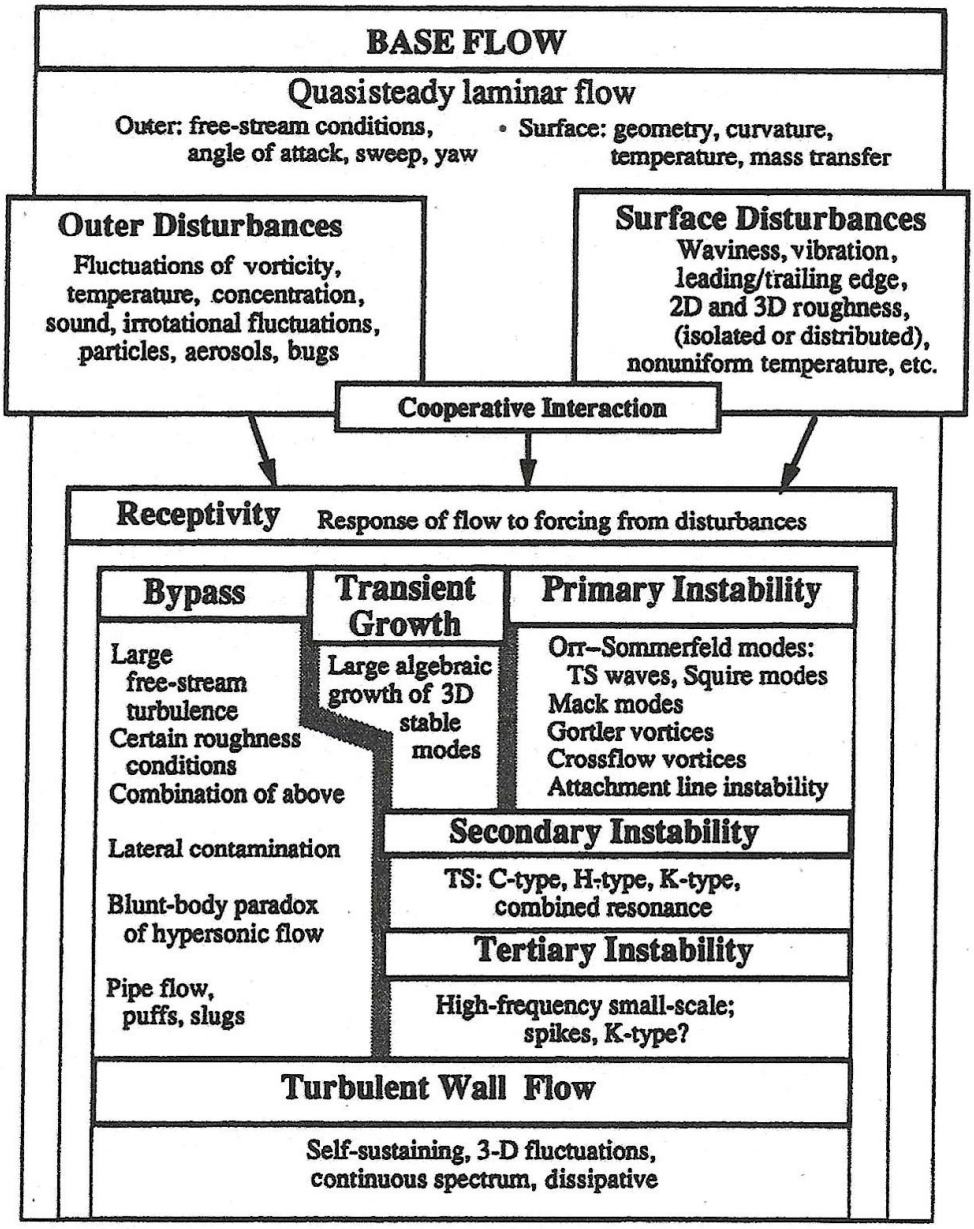

Figure 25.11 Morkovin map of the roads to wall turbulence.

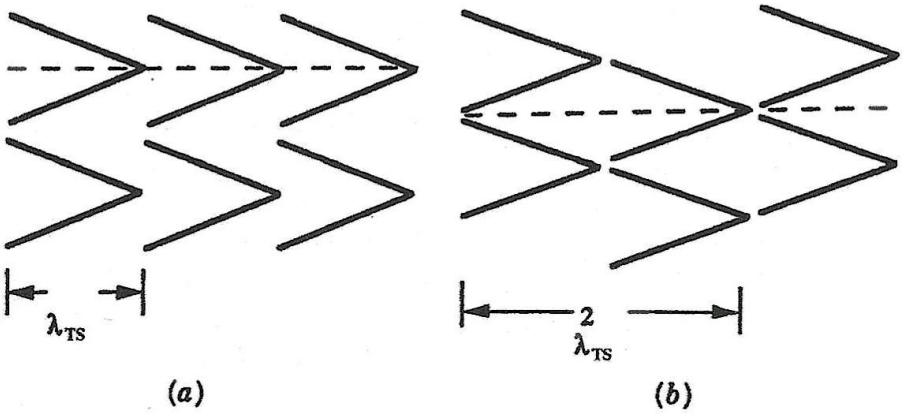

Figure 25.12 Secondary instabilities of TS waves: (*a*) aligned mode, $\varepsilon = 0$; (*b*) staggered mode, $\varepsilon = 1$.

Spatially Developing Open Flows

Temporal OS analysis: α real and $c = c_R + ic_I$ investigates the local stability of nearly parallel flow profiles.

Spatial stability analysis: c real and $\alpha = \alpha_R + i\alpha_I$ also investigate local stability.

More generally both time and space instability are investigated via insertion of an impulse into the flow.

Locally convectively unstable: perturbation grows and swept downstream such that unperturbed main flow remains. BL flows.

Locally absolutely unstable: disturbance grows at a fixed position. Mixing layer flows.

Globally instability: Karman vortex street via elliptic nature incompressible NS induces pressure signals that affect upstream flow and vortex formation.

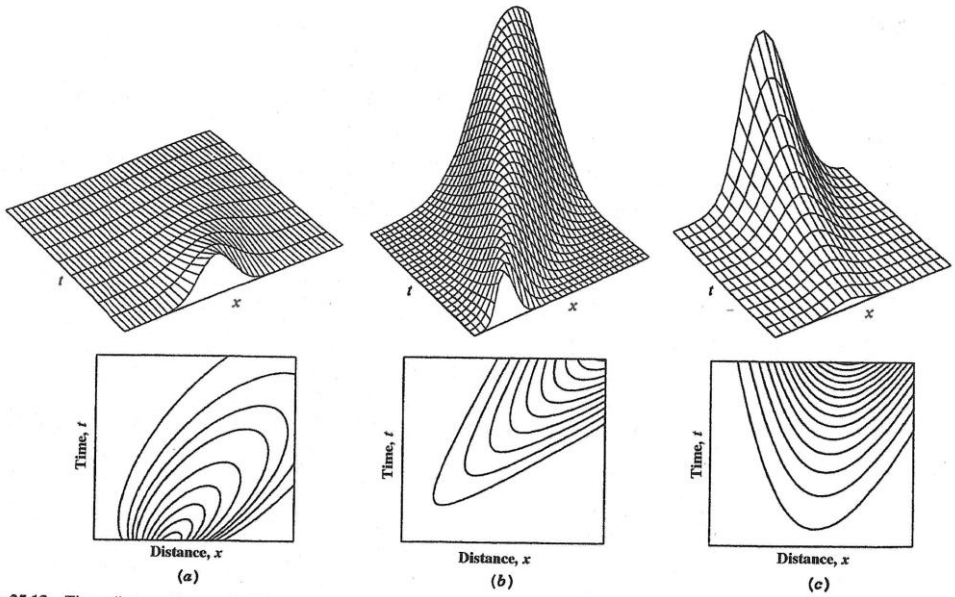

Figure 25.13 Time–distance history of a disturbance. Flow is left to right: (*a*) stable, (*b*) convectively unstable, and (*c*) absolutely unstable. Courtesy of L. Paulon and P. A. Monkewitz, *École* Polytechnique Federale de Lausanne. Reprinted with permission.

Transition in Free Shear Flows

Free shear flows are subject KH inviscid instability, which grows rapidly to amplitudes where nonlinearities are important.

Nonetheless OS theory predicts the initial process with better success spatial vs. temporal analysis.

Linear theory predicts the most amplified frequency f_n, which only lasts a short distance (about eight wave lengths) from the splitter plate after which a subharmonic $f_n/2$ dominates explained by secondary instability theory.

Jets are initially shear layers near their exit, which merge, and the flow becomes spatially developing requiring global instability analysis.

Poiseuille and Plane Couette Flows. Appendices B and C.

The linear OS theory fails for plane Couette flow and pipe Poiseuille flows, as it predicts compete stability, whereas for sufficient Re these flows undergo transition. It also fails for plane Poiseuille flows in that it predicts transition at Re much larger (about 6 times) experimental value.

Pipe flows show a variety of critical Re depending experimental/numerical setup. Nominally Re = 2000 is used; however, laminar flow has been attained for Re up to 40K and plane Couette flow has become unstable with Re as low as 360. Plane Poiseuille has been studied extensively due to its geometric simplicity.

OS indicates Re critical 5772 (based on h/2) but experiments become turbulent with Re as low as 1K or as high as 8K with in both cases very slow growth rates and observable TS waves.

Although no complete theory exists, the main themes are 2D nonlinear (with average shear stress and pressure gradient unchanged), 3D secondary instability, and 3D transient growth, as per Fig 25.14.

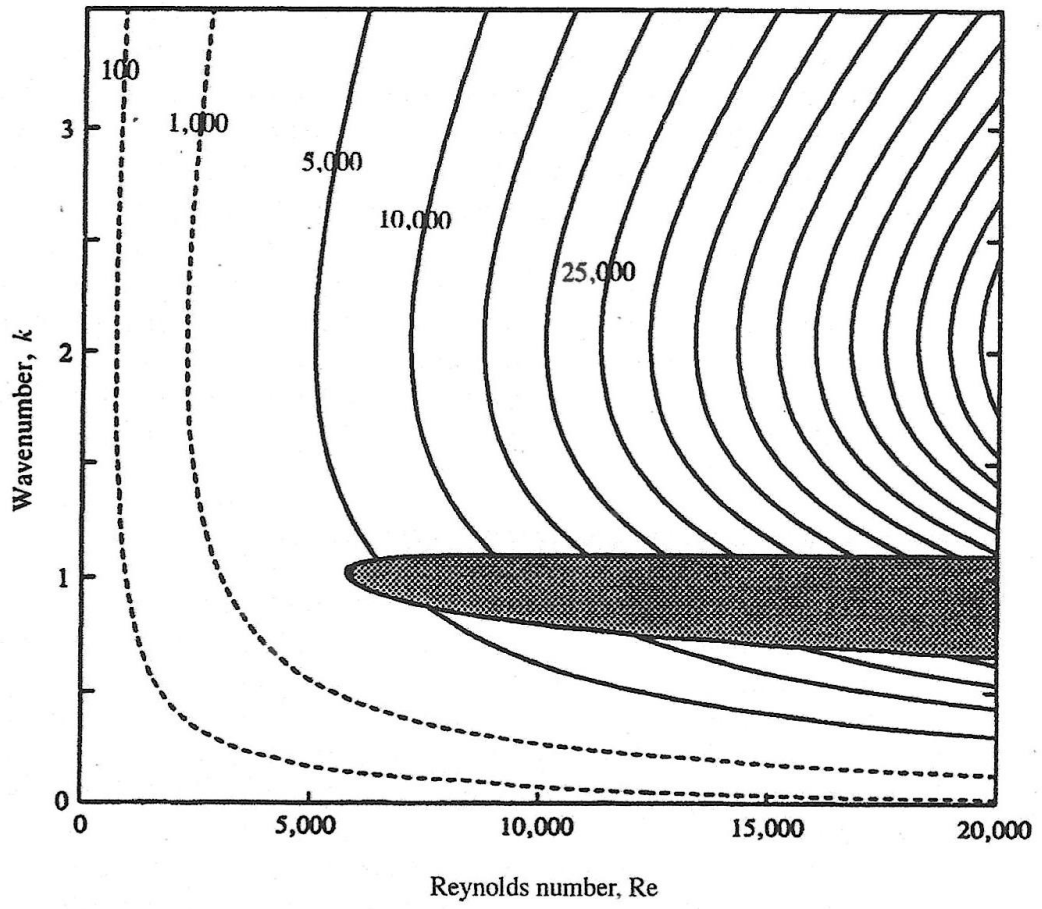

Figure 25.14 Transient growth in plane Poiseuille flow. Contour lines depict the maximum energy growth factors for a disturbance. Here the wavenumber is $k = \sqrt{\alpha^2 + \beta^2}$. The shaded area is unstable for TS waves. This is a different version of the amplification factor map of Trefethen et al. (1993).